# Influence of alkyl side-chain type and length on the thin film microstructure and OFET performance of naphthalene diimide-based organic semiconductors

Adam Welford[a], Subashani Maniam[b], Eliot Gann[a,c,1], Xuechen Jiao,[a,c] Lars Thomsen[c], Steven J. Langford[d], Christopher R. McNeill[a,*]

[a]Department of Materials Science and Engineering, Wellington Road, Clayton, Victoria, 3800, Australia
[b]School of Chemistry, Monash University, Wellington Road, Clayton, Victoria, 3800, Australia
[c]Australian Synchrotron, ANSTO, 800 Blackburn Road, Clayton, Victoria, 3168, Australia
[d]Department of Chemistry and Biotechnology, Swinburne University, John St, Hawthorn, Victoria, 3122, Australia

[*]Corresponding author.
*Email address:* christopher.mcneill@monash.edu (C.R. McNeill)
[1]Present address: Materials Science and Engineering Division, National Institute of Standards and Technology, Gaithersburg, MD 20899, USA.

## ABSTRACT

Here we study the effect of side chain length and type on the microstructure and organic field-effect transistor (OFET) performance of solution-processed naphthalene diimide (NDI) thin films. Linear side chains with four (C4), five (C5), six (C6), eight (C8) and twelve (C12) carbon atoms are studied along with a branched ethyl hexyl (EH) side chain. Interestingly, mobilities of up to ~ 0.2 $cm^2/Vs$ are achieved for short (C4) and long (C12) side chains with linear chains of intermediate length and the branched side chain producing lower mobilities. The observed mobility trends are explained in terms of the competing influence of changes in crystal packing and changes in thin film morphology with changes in side chain length. Shorter side chains produce changes in the lateral stacking of NDI units which promote higher mobility while longer side chains produce solution-processed thin films with higher film quality evidenced by larger domain sizes and lower orientational disorder. Side chain length is also found to strongly modulate the molecular orientation of the NDI core, with high edge-on orientations observed for long chains, and tilted orientations for short chains. Thin film microstructure is investigated using a range of techniques including atomic force microscopy, grazing incidence wide-angle X-ray scattering and near-edge X-ray absorption fine-structure spectroscopy.

*Keywords:* OFETs, Naphthalene diimides, Thin films, Organic semiconductors, Microstructure

## 1. Introduction

Organic semiconductors continue to attract interest for application in a wide-range of technologies. Organic light emitting diode (OLED) displays based on sublimed organic semiconductors have been widely commercialised, with other technologies based on organic field effect transistors (OFETs) and organic solar cells at varying stages of commercialisation. OFETs in particular have the potential to lead to new commercial products based on attractive properties such as mechanical flexibility, novel form factors, sensitivity to analytes, and potential low cost of manufacture [1]. These properties make OFETs appealing for application in devices such as flexible displays, sensors, and radio frequency identification (RFID) [2-4]. Organic semiconductors can be broadly categorised into two main classes: conjugated polymers and so-called small molecules, although macromolecular dendrimers combine properties of both classes [5]. Conjugated polymers are generally processed from solution, while small molecules can either be deposited via solution processing or by vapour deposition. Flexible side chains are typically required to enable solution processability, since the active semiconducting component of organic semiconductors are planar aromatic units which have a strong tendency to aggregate via π-stacking. As well as enabling solution processability, these flexible side chains strongly affect molecular packing, with "side-chain engineering" an important strategy to optimise the performance of solution-processed organic semiconductors [6]. Many different types of side chains can be employed, including alkylated, conjugated, ionic and fluoroalkylated side chains [7]. Other properties of the side chain including the geometry (e.g. branched vs. linear), the bulkiness and attachment density can also be important [8, 9]. Alkyl side chains have been the most widely employed class of side chain. Within the class of alkyl side chains, linear, branched and cyclic alkyl chains have been utilised, with properties such as alkyl side chain length and side chain branching position found to be key parameters [10]. While side-

chain engineering has been widely employed for conjugated polymers [11, 12], there have been fewer side-chain engineering studies on solution processed small molecules [13, 14]. Compared to conjugated polymers, small molecules show a higher degree of molecular order making them attractive for being able to directly associate changes in side chain properties with thin film microstructure and charge transport.

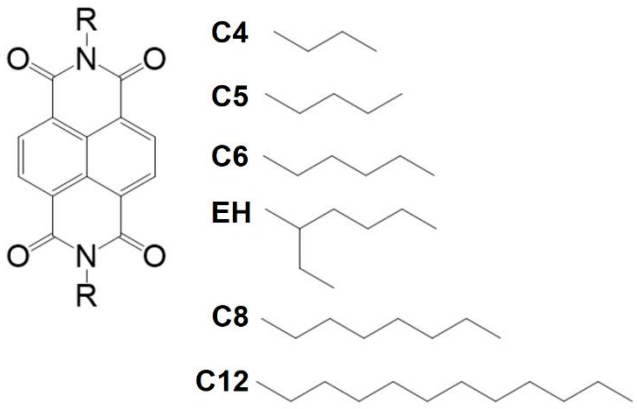


Figure 1. Chemical structures of the NDI derivatives used in this study.

The naphthalene diimide (NDI) moiety is an important building block used for the realisation of high mobility *n*-type materials, both small molecule and polymeric [15]. Being the smallest of the rylene diimides, it possess a relatively deep lowest unoccupied molecular orbital (LUMO) due to the strong electron withdrawing properties of the imide groups. Solution processability is enabled by substituting solubilising side chains to the nitrogen atoms. Core functionalisation [16] and core expansion [17] enable further tuning of the NDI framework, while the co-polymerisation of NDI units with electron rich units has resulted in high performance *n*-type donor-acceptor copolymers [18]. A mobility of up to 8.6 $cm^2/Vs$ has been achieved for ribbon-shaped single crystals of a core-chlorinated derivative [16] while a mobility of 6 $cm^2/Vs$ has been achieved for a cyclohexyl-substituted NDI derivative processed via vacuum sublimation [19]. Lower mobilities are typically achieved for solution-processed NDI derivatives. Although a mobility of up to 3.5 $cm^2/Vs$ has been achieved for

solution-processed core-expanded NDI derivatives [20], the mobilities achieved for solution-processed NDI derivatives are generally less than 1 $cm^2/Vs$ [21], especially for NDI molecules without core functionalisation or core expansion [22, 23]. Although NDI molecules with a wide range of different side chains have been reported [22-31], there have been few systematic studies on how variations of the side chain length and type affect the microstructure and performance of solution processed layers. A recent theoretical study by Ma et al. has investigated the effect of alkyl side-chain length on molecular packing and carrier mobility [32]. Ma et al. calculated the charge transport mobility of NDI derivatives and predicted that it should decrease with increasing alkyl chain length due to displaced stacking along the short axis of the π-π stacked molecules [32]. This study suggested that short alkyl side chains should be beneficial for charge transport. Here we experimentally investigate how side chain length and type affects the microstructure and charge transport properties of solution processed NDI thin films. The set of molecules studied is shown in Figure 1, with side chain length spanning butyl (NDI-C4) to dodecyl (NDI-C12), largely coinciding with the set of molecules studied by Ma et al. [32] We also include in our study a derivative with branched ethylhexyl side chains to study the influence of branched vs. linear side chains. Thin film microstructure is characterised with atomic force microscopy (AFM), grazing incidence wide-angle X-ray scattering (GIWAXS) and near-edge X-ray absorption fine-structure (NEXAFS) spectroscopy. Together these techniques enable the morphology, thin film crystallinity and molecular orientation of solution processed thin films of these NDI derivatives to be characterised. OFET characteristics are also reported to enable comparison between thin film microstructure and charge transport. While Ma et al. calculated that mobility should decrease with increasing alkyl chain length, we find a more complicated relationship for charge transport in solution-process thin films. In general, longer side chains (NDI-C12) are found to produce higher quality thin films enabling mobilities of up to 0.2

$cm^2/Vs$. Relatively high mobilities of $\geq 0.1$ $cm^2/Vs$ can also be achieved with shorter chains (NDI-C4, NDI-C5), where the mobility is limited by microstructural imperfections. Interestingly the lowest mobilities were found for NDI-C6 and NDI-EH which is attributed to the presence of multiple polymorphs. A strong relationship is found between chain length and molecular orientation. The properties of spin-coated and blade-coated films are also compared.

## 2. Materials and methods

### *2.1 Synthesis*

The chemical synthesis of the NDI materials used in this study, Figure 1, has been previously reported and can be found elsewhere [33, 34].

### *2.2 Transistor fabrication*

Transistors were fabricated with a top-gate bottom-contact geometry. Gold electrodes were used for source and drain electrodes, patterned via photolithography onto silicon-oxide coated silicon wafers which were used as the substrate. Source-drain electrodes were patterned with an interdigitating pattern, with a channel length of $L$ = 20 μm and channel width of $W$ = 10 mm. The thickness of the gold source-drain electrodes was 15 nm with an underlying 5 nm thick chromium adhesion layer. After solvent cleaning and oxygen plasma cleaning, the gold source-drain electrodes were coated with a very thin (< 5 nm) layer of ethoxylated polyethylenimine (PEIE) which was spin-coated from a 2-methoxymethanol solution (0.01 wt.%). Substrates were then placed on a hotplate at 110°C to dry and crosslink the PEIE. The purpose of this PEIE layer is to facilitate electron injection, with PEIE altering the work function of gold from ~ 3.9 eV to 5.1 eV [35]. The active semiconducting layer was next deposited either by spin-coating or blade-coating. Chlorobenzene was used as the solvent, with a solution concentration of 10 mg/mL used. Spin-coating was performed using solutions heated to 80°C and coating at 2000 rpm. Blade coating was performed using a

home-built blade coater based on a system described elsewhere [36]. For blade coating a solution temperature and substrate temperature of 100°C was used, with a coating speed of 10 mm/s employed. The semiconducting layer was then annealed under nitrogen at 60°C for 45 minutes prior to coating with the amorphous fluorinated dielectric CTYOP (500 nm thick). An aluminium gate electrode completed the device, evaporated through a shadow mask.

*2.3 Transistor characterisation*

Transistor characterisation was carried out in a nitrogen-filled glove box. A Signatone H150 probe station was used to contact the devices, and electrical characterisation performed with a 2 channel source measure unit (Agilent B2900A). Processing of transistor data was performed with the assistance of custom scripts written in Igor Pro to determine the saturation mobility (μ) and threshold voltage ($V_{th}$) from plots of the square root of the drain current ($I_d$) vs. the gate voltage ($V_g$). In particular, according to the gradual channel approximation, under saturation conditions:

$$I_d = \mu\left(\frac{WC_i}{2L}\right)\left(V_g - V_{th}\right)^2 \quad (1)$$

where $C_i$ is the areal capacitance. Hence μ was calculated from the slope of $I_d^2$ vs. $V_g$.

*2.4 Atomic force microscopy (AFM)*

Samples were prepared on PEIE treated $Si/SiO_2$ wafers. AFM images were acquired using ScanAsyst mode using a Bruker Dimension Icon AFM at the Melbourne Centre for Nanofabrication (MCN) facility. AFM images were processed and analysed using Gwyddion data analysis software to acquire layer step heights of the NDI samples.

*2.5 Grazing-incidence wide-angle X-ray scattering*

GIWAXS measurements were performed at the SAXS/WAXS beamline of the Australian Synchrotron [37]. Samples were prepared on PEIE-treated $Si/SiO_2$ wafers to

match transistor fabrication. Highly collimated 11 keV X-ray photons were aligned parallel to the substrates by varying sample height and polar angle while measuring the transmitted signal with a crystal analyser. 2D GIWAXS patterns were recorded on a Dectris Pilatus 1M detector with each 2D scattering pattern being the result of a total of 3 s of exposure. Three 1 second exposures were taken at different lateral detector positions to fill in the gaps between modules in the detector, and combined in software. Angular steps of 0.01° were taken near the critical angle, in order to determine the angle of maximum scattered intensity. The sample to detector distance was measured using a silver behenate scattering standard. A modified version of the NIKA [38] small angle scattering analysis package was used to analyse the data, with peak fitting performed using least squares multipeak fitting within IgorPro.

*2.6 Near-edge x-ray absorption fine-structure spectroscopy*

NEXAFS spectroscopy was performed at the Soft X-ray beamline at the Australian Synchrotron, ANSTO [39], using an X-ray beam with near perfect linear polarisation. Carbon K-edge spectra were measured from ~ 270 eV to 330 eV, with X-ray absorption recorded via the detection of energetic electrons emitted from the sample with a channeltron detector (partial electron yield mode). The incident X-ray flux was monitored with a gold mesh upstream from the sample, with carbon contamination on the mesh quantified via measurement of the direct beam intensity with a photodiode. Spectra were double normalised to the incident photon flux and processed using the QANT software package [40] implemented in Igor Pro. Molecular orientation was quantified by determination of the average tilt angle, γ, of the C 1s to π* transition dipole moment (TDM) using the equation

$$I \propto \frac{1}{3}\left[1 + \frac{1}{2}(3\cos^2\theta - 1)(3\cos^2\gamma - 1)\right] \quad (2)$$

where *I* is the resonance intensity and θ is the X-ray angle of incidence. Further details regarding data acquisition and data processing can be found elsewhere [41].

## 3. Results

### *3.1 Atomic force microscopy*

Six NDI derivatives were studied, five with linear side chains, and one with a branched, ethylhexyl side chain (NDI-EH). Linear side chains spanned from butyl (NDI-C4) to dodecyl (NDI-C12) in length, with pentyl (NDI-C5), hexyl (NDI-C6) and octyl (NDI-C8) in between. Figure 2 presents AFM images of spin-coated and blade coated films of the six different molecules. In general, the spin-coated films exhibit much rougher topographies. There are differences in the morphology of the spin-coated films across the series of six molecules. NDI-C4 and NDI-C6 appear to exhibit platelet-like structures, with NDI-C6 in particular exhibiting a rather disordered stacking of platelets that are oriented at different angles to the substrate. NDI-C5 in contrast appears to exhibit a locally smoother topography but with larger structures and cracks. The reason for the different behaviour of NDI-C5 is not clear; the odd number of carbon atoms (as opposed to the even number of carbon atoms in the other samples studied) could influence the packing behaviour [42] and future studies including more odd-numbered chains could provide light on this possibility. NDI-EH shows a more nodular morphology with the presence of elliptical structures a micron or so is diameter. NDI-C8 and NDI-C12 appear to show a more uniform, ordered packing of molecules, with molecular terraces evidence in the AFM image of the spin-coated NDI-C12 film. Ordered molecular terracing is clear in all of the blade-coated samples, indicating that the solution coating method used can have a significant influence of the resulting thin-film morphology. Similar uniform terraced morphologies have been observed by Ichikawa et al. for NDI-C11, NDI-C12 and NDI-C13 by melt annealing subsequent to spin-coating [22]. Here it is shown that such morphologies can be produced by blade coating without recourse

to melt annealing, which Ichikawa et al. found to be problematic for NDI derivatives with shorter side chains [22]. The quality and uniformity of the blade-coating layers improves with increasing alkyl chian length, with blade-coated NDI-C12 films exhibiting uniform terracing and large terraced domains. From the molecular terracing observed in the AFM images of the blade-coated samples it is possible to extract the molecular terrace height, which is summarised in Table 1. The measured molecular step height as a function of alkyl chain length is found to systematically increase from 1.15 nm for NDI-C4, to 1.33 nm for NDI-C5, 1.47 nm for NDI-C6, 1.70 nm for NDI-EH, 2.18 nm for NDI-C8 and 2.83 nm for NDI-C12. Interestingly NDI-EH with branched ethylhexyl side chains exhibits a larger step height compared to NDI-C6 which has linear side chains of the same length, indicating that side chain branching leads to an expansion along the long axis of the molecule.

Table 1. Summary of molecular step height values extracted from the AFM data, and molecular orientations extracted from NEXAFS spectroscopy.

| Material | Step Height from AFM (nm) | NEXAFS Tilt Angle, γ | |
|---|---|---|---|
| | | Spin-coated | Blade-coated |
| NDI-C4 | 1.15 ± 0.05 | 52.2° ± 0.2° | 52.5° ± 0.2° |
| NDI-C5 | 1.33 ± 0.05 | 54.4° ± 0.3° | 51.6° ± 0.3° |
| NDI-C6 | 1.47 ± 0.05 | 57.8° ± 0.3° | 64.1° ± 0.5° |
| NDI-EH | 1.70 ± 0.05 | 55.3° ± 0.4° | 55.4° ± 0.4° |
| NDI-C8 | 2.18 ± 0.05 | 77.7° ± 0.9° | 77.5° ± 0.8° |
| NDI-C12 | 2.83 ± 0.05 | 89.0° ± 1.0° | 83.9° ± 0.9° |

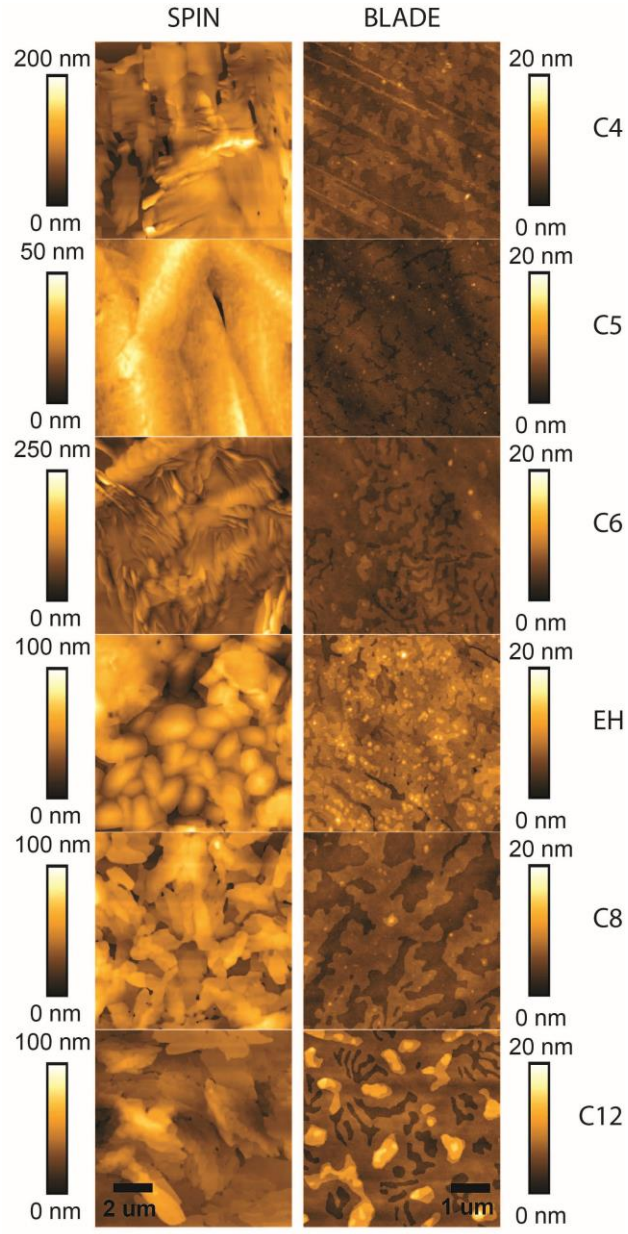


Figure 2. Surface topography of spin-coated (left) and blade-coated films.

*3.2 Grazing incidence wide-angle X-ray scattering*

Figure 3 presents the two-dimensional grazing incidence wide-angle X-ray scattering (GIWAXS) images taken of spin-coated and blade-coated films. All films exhibit highly crystalline microstructures with a high degree of texture, albeit with varying degrees. Broadly comparing the spin-coated and blade-coated data, the GIWAXS patterns of the blade-coated samples show less ‘arcing’ of the peaks indicative of a higher degree of texture or lower

degree of mosaicity. In other words, the spin-coated samples show a large spread of the orientation of crystalline planes in the films; this is in agreement with the AFM data where the spin-coated samples in general are rougher and more angular in morphology. The diffraction patterns from the blade-coated samples appear weaker which is due to the thinner thickness of the blade-coated samples. Comparing samples with different side chain lengths, samples with shorter side chains exhibit a larger degree of mosaicity. Longer side chain samples exhibit very little arcing of peaks consistent with the flatter AFM morphologies of these samples.

For each molecule we have attempted to index the unit cells. NDI-C4, NDI-C5, NDI-C8 and NDI-C12 all can be indexed to a single triclinic unit cell, while NDI-C6 and NDI-EH exhibit more complicated scattering patterns attributed to the presence of at least two polymorphs. For all materials, the same crystal structures are observed for spin-coated vs. blade coated samples, although in the case of NDI-C6 and NDI-EH the second polymorph is less pronounced. Table 2 summaries the unit cell parameters, with the *c*-axis indexed as the longest axis corresponding to the side-chain stacking direction of the molecules. These NDI molecules tend to pack with a cofacial π-π stacking with layers of the conjugated core separated by layers of alkyl side chains [32]. The length of the *c*-axis is therefore related to the length of the alkyl side chains, see Figure 4, with good agreement between the values determined for the *c*-axis spacing and the molecular terrace heights measured by AFM. For example, the *c*-axis of NDI-C4 is 1.10 nm from the X-ray data compared to 1.15 nm from the AFM data, and the *c*-axis of NDI-C12 is 2.89 nm from the X-ray data compared to 2.83 nm from the AFM data. The fact that the *c*-axis is oriented along the $Q_z$ direction for all samples also indicates that the molecules are adopting an ‘edge-on’ orientation with respect to the substrate.

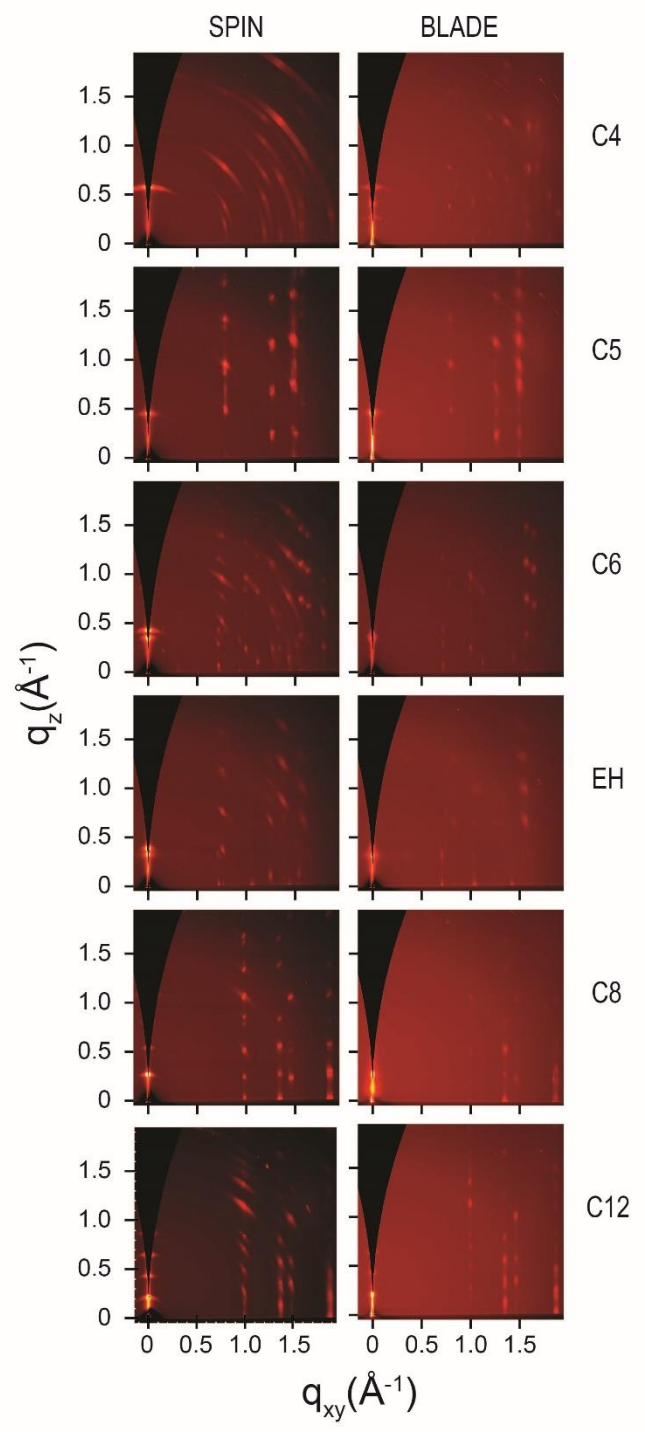


Figure 3. Two dimensional GIWAXS images of spin-coated (left) and blade-coated (right) films.

Table 2. Summary of the unit cell parameters determined from the 2D GIWAXS images.

| Material | *a* (Å) | *b* (Å) | *c* (Å) | α (°) | β (°) | γ (°) | Unit Cell Volume (Å$^3$) |
|---|---|---|---|---|---|---|---|
| NDI-C4 | 8.1 | 5.4 | 11.0 | 95.6 | 104.5 | 94.1 | 463 |
| NDI-C5 | 8.0 | 5.0 | 13.6 | 99.6 | 93.2 | 90.0 | 531 |
| NDI-C6[a] | 8.3 | 5.7 | 14.4 | 90 | 96.5 | 96 | 673 |
| NDI-C6[b] | 8.8 | 6.7 | 17.7 | 90.5 | 97 | 84 | 1030 |
| NDI-EH[a] | 18.0 | 8.5 | 19.83 | 90.9 | 90.7 | 90.6 | 3010 |
| NDI-EH[b] | 17.2 | 11.2 | 16.89 | 95.1 | 92.0 | 88.5 | 3244 |
| NDI-C8 | 6.6 | 4.5 | 22.6 | 88.7 | 92.2 | 105.2 | 693 |
| NDI-C12 | 6.5 | 4.5 | 28.9 | 95.4 | 91.9 | 105.8 | 875 |

[a]Primary polymorph. [b]Secondary polymorph.

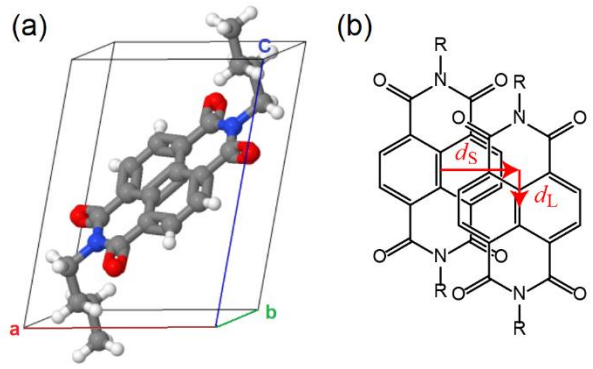


Figure 4. (a) Schematic showing a likely orientation of an NDI molecule within the unit cell. The case shown here is for NDI-C5 based on the single crystal structure published by Alvey et al. [43]. (b) Definition of $d_S$ and $d_L$ in terms of the displacement of neighbouring NDI molecules along the short and long axes respectively.

While the size of the *c*-axis shows a systematic increase in size with increasing chain length – consistent with the AFM data – the trends in the values of the *a*- and *b*- axes are more subtle. In general the length of both the *a*- and *b*-axes decrease going from NDI-C4 to NDI-C12, with the value of the *a*-axis decreasing from 8.1 Å for NDI-C4 to 6.5 Å for NDI-C12, and the value of the b-axis decreasing from 5.4 Å for NDI-C4 to 4.5 Å for NDI-C12. These changes can be seen as reflecting changes in the molecular packing of the molecule

within the unit cell. A change in the value of the *a*-axis is more likely to reflect a change in displacement along the short axis of the molecule, $d_S$, while a change in the value of the *b*-axes is more likely to reflect a change in the π-π stacking distance, $d_P$, and tilting of the molecule within the unit cell. (Changes in the value of the *c*-axis will also be influenced by changes in displacement along the long axis of the molecule, $d_L$, however such changes will be small compared to the changes seen due to changes in side chain length.) Thus as the length of side chain increases from C4 to C12 the displacement of the NDI core along the short axis of the molecule decreases, while the separation of the molecules along the *b*-axis shortens. This decrease in the displacement along the short axis is consistent with the modelling of Ma et al. who calculated that the displacement along the short axis, $d_S$, decreases from 3.8 Å for NDI-C4 to 2.8 Å for NDI-C12 [32]. Their calculations did not show much change in the perpendicular distances between planes of NDI monomers, $d_P$, with this value remaining relatively constant at $d_P$ = 3.3 Å for all derivatives studied. The changes in the size of the *b*-axis are then likely to be due to changes in the molecular orientation of the molecules: changes in the tilting of the NDI core within the unit cell will produce changes in the value for *b* in the absence of a change in $d_P$. Indeed systematic changes of the molecular orientation of the NDI core are confirmed by NEXAFS spectroscopy, see below. While there is an overall decrease of the size in the *a*-axis and *b*-axis from NDI-C4 to NDI-C12, this change is not systematic; these values remain similar (or even increase slightly) for NDI-C4 to NDI-C6 before dropping significantly going for NDI-C6 to NDI-C8. Thus this trend would seem to indicate a more abrupt transition for side chain lengths greater than six carbon atoms. The molecular packing of NDI-EH with branched side chains is clearly more complicated with more than one molecule per unit cell. Further insight into the effect of side-chain length on molecular packing could be achieved by crystallographic refinement calculations to

accurately determine the position of the molecules within the unit cell [44], however these calculations are rather specialised and beyond the scope of this work.

*3.3 Near-edge X-ray absorption fine-structure spectroscopy*

Complementary to GIWAXS, NEXAFS spectroscopy is able to probe the molecular orientation of organic molecules in thin films. NEXAFS spectroscopy is a synchrotron-based X-ray absorption spectroscopy technique which measures absorption corresponding to transitions from a core state to antibonding states. In carbon K-edge NEXAFS spectroscopy, as employed here, transitions from the carbon 1s orbital to antibonding $\sigma^*$ and $\pi^*$ states are probed. The lowest energy features at around 284 eV to 286 eV are due to 1s $\rightarrow$ $\pi^*$ transitions, with the resonance intensity for this transition related to the orientation of the transition dipole moment (TDM) relative to the electric field vector of the polarised X-ray beam. By measuring angle-resolved spectra, where the incident angle of the X-ray beam is changed relative to the substrate, the molecular orientation of the conjugated NDI core can be determined. Further details regarding the use of NEXFAS spectroscopy to study organic thin films can be found elsewhere [45]. Figure 5 presents the angle-resolved NEXAFS spectra of both spin-coated and blade-coated films. Examining the dichroism of the 1s $\rightarrow$ $\pi^*$ transitions (highlighted by the insets) the highest dichroism is seen for NDI-C8 and NDI-C12, where the peak intensity of the $\pi^*$ peaks for grazing incidence (20°) are much lower than that for normal incidence (90°). This observation is consistent with an edge-on orientation of the NDI core, with the 1s $\rightarrow$ $\pi^*$ TDM oriented in the plane of the sample (the 1s $\rightarrow$ $\pi^*$ is oriented perpendicular to the planar conjugated core). Using equation 2 average tilt angle values for the 1s $\rightarrow$ $\pi^*$ TDM for NDI derivative have been calculated and are tabulated in Table 1. A tilt angle of 90° corresponds to a perfectly edge-on orientation of molecules with respect to the substrate whereas a tilt angle of 0° corresponds to a perfectly face-on (lying flat) orientation

of molecules. It is important to note that the tilt angle measured by NEXAFS is different to the orientation of the unit cell probe by GIWAXS. NEXAFS directly probes the tilting of the orientation of the NDI core, and since the NDI core can tilted within the unit cell a highly textured film with (00l) axis oriented perpendicular to the substrate can still exhibit a tilt angle of less than 90°. Examining the NEXAFS data, a systematic increase in tilt angle for the linear series of molecules can be seen, with γ increasing from ~ 52° for NDI-C4 to well over 80° for NDI-C12. Since the blade coated samples in general show a high degree of texture from GIWAXS measurements and molecular terracing from AFM measurements, the tilt angles measured for the blade coated films are representative of the preferential molecular orientation of the NDI core within the unit cell. The increase in tilt angle from ~ 52° for NDI-C4 to ~ 85° for NDI-C12 is thus consistent with the decrease in the size of the *b*-axis measured by GIWAXS as the molecule stands more upright in the unit cell. Comparing the tilt angles derived from the spin-coated and blade-coated samples, in general similar average tilt angles are found in both cases. For NDI-C4 and NDI-C5 average tilt angles of γ ~ 52° to 55° are found which are close to the 'magic angle' of 54.7° which could either correspond to a preferential orientation of 54.7° or a random distribution of tilt angles. From the AFM images, the topography of the NDI-C4 and NDI-C5 films are rougher compared to the blade coated films, however this may not affect the average tilt angle since the values are close to the magic angle. For NDI-C6, a significantly lower tilt angle of γ ~ 58° is measured compared to γ ~ 64° for the blade-coated sample which is consistent with the rougher surface topography and tilted crystallites seen with AFM. For NDI-C8 and NDI-C12 relatively flat surface topographies are seen in the spin-coated AFM images helping to explain the similar tilt angle observed for spin-coated and blade-coated NDI-C8. For NDI-EH with branched side chains, tilt angles of ~ 55° are found for both spin-coated and blade-coated films.

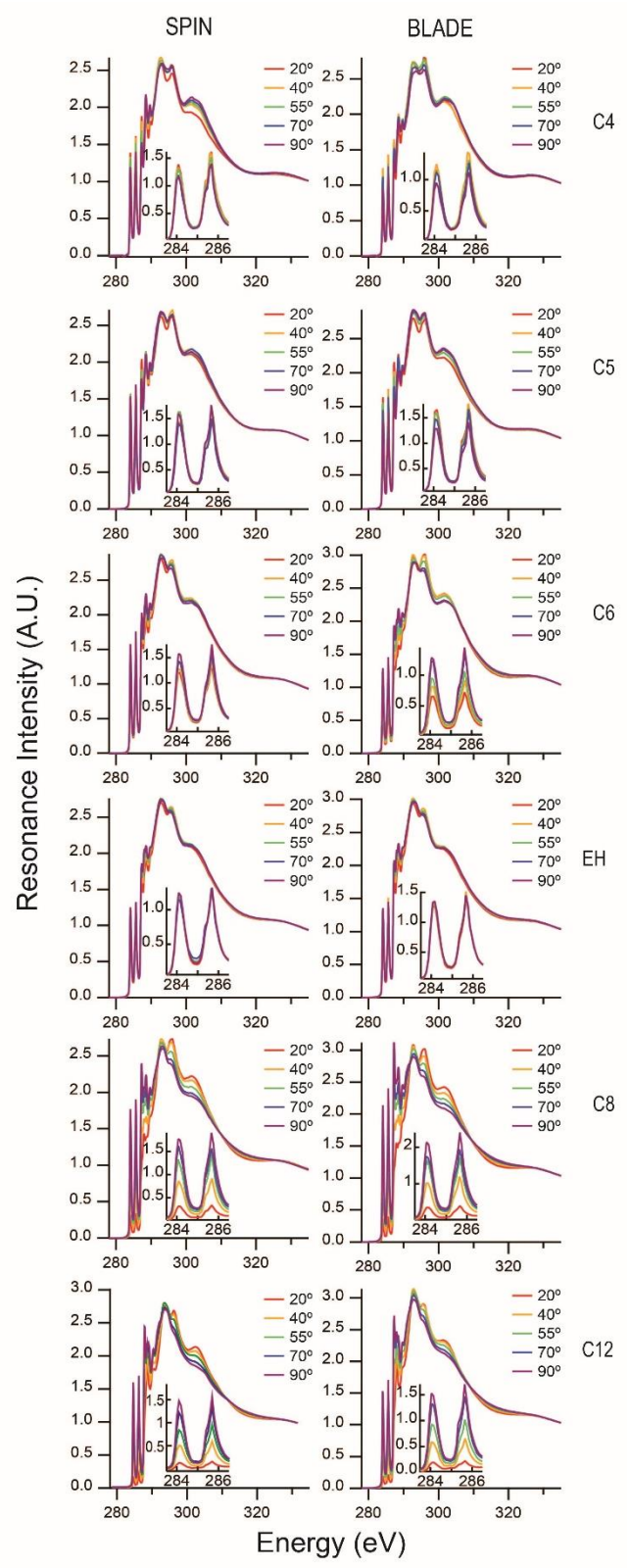


Figure 5. NEXAFS spectroscopy of spin-coated (left) and blade-coated (right) films of the NDI derivatives studied.

*3.4 Transistor data*

Typical output and transfer curves for blade-coated OFETs are shown in Figure 6. Transistor data for spin-coated OFETs are shown in the supplementary data. All OFETs show well-defined transistor characteristics with clean transfer characteristics enabling reliable determination of saturation mobility from the slope of the $I_D^{½}$ vs. $V_G$ curves. OFET parameters extracted from the transfer characteristics are summarised in Table 3, including the saturation electron mobility, threshold voltage and I on/off ratio. In general high electron mobilities are achieved for blade-coated samples consistent with the more favourable morphology of these films. Mobilities of up to ~ 0.2 $cm^2$/Vs are achieved for both NDI-C12 and NDI-C4, with lower mobilities achieved for intermediate chain length. Looking at the trend with chain length, the mobility for blade-coated OFETs drops from 0.18 $cm^2$/Vs for NDI-C4, to 0.1 $cm^2$/Vs for NDI-C5, to 0.06 $cm^2$/Vs for NDI-C6 before increasing again to 0.12 $cm^2$/Vs for NDI-C8 and to 0.19 $cm^2$/Vs for NDI-C12. NDI-EH with branched side chains also shows a relatively low mobility of ~ 0.07 $cm^2$/Vs. The lowest threshold voltages are observed for NDI-C8 and NDI-C12 which could be due to the favourable surface topography of these films which minimise charge trapping.

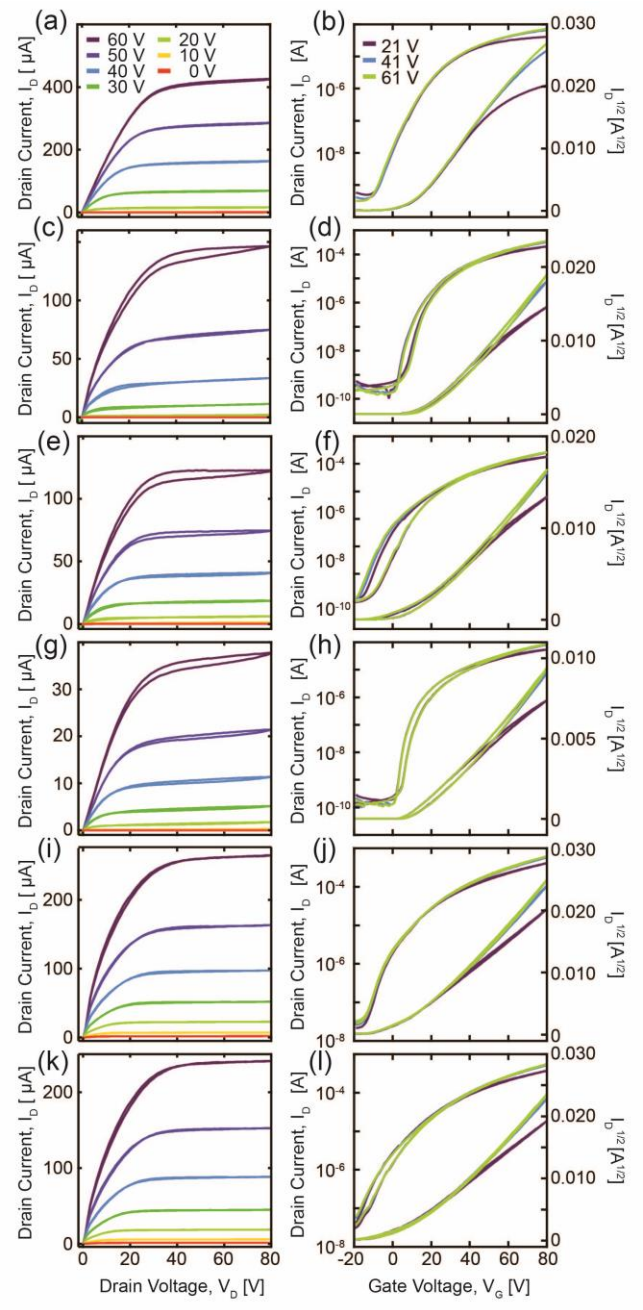


Figure 6. Output (a, c, e, g, i, k) and transfer (b, d, f, h, j, l) of blade-coated OFETs based on NDI-C4, (a, b), NDI-C5, (c, d), NDI-C6, (e, f), NDI-EH, (g, h), NDI-8H, (i, j), and NDI-C12, (k, l).

Table 3. Summary of the device parameters of spin-coated (SC) and blade-coated (BC) top gate bottom contact (TGBC) OFETs based on the six NDI derivatives studied. Values reported are average values from at least 8 transistors.

| Material | | Electron mobility ($cm^2/Vs$) | Threshold Voltage (V) | I on/off ratio |
|---|---|---|---|---|
| NDI-C4 | SC | 0.070 ± 0.01 | 2.5 ± 1.0 | $10^4$ |
| | BC | 0.18 ± 0.03 | 7.7 ± 1.1 | $10^5$ |
| NDI-C5 | SC | 0.10 ± 0.01 | 30 ± 3.0 | $10^4$ |
| | BC | 0.10 ± 0.02 | 22 ± 1.6 | $10^5$ |
| NDI-C6 | SC | 0.014 ± 0.002 | 6.2 ± 0.8 | $10^4$ |
| | BC | 0.060 ± 0.002 | 11 ± 3.5 | $10^5$ |
| NDI-EH | SC | 0.028 ± 0.003 | 20 ± 2.0 | $10^5$ |
| | BC | 0.068 ± 0.006 | 12 ± 4.0 | $10^4$ |
| NDI-C8 | SC | 0.11 ± 0.01 | -4.2 ± 1.0 | $10^6$ |
| | BC | 0.12 ± 0.02 | -4.2 ± 0.7 | $10^5$ |
| NDI-C12 | SC | 0.15 ± 0.01 | -2.3 ± 0.9 | $10^6$ |
| | BC | 0.19 ± 0.02 | -2.0 ± 1.0 | $10^5$ |

## 4. Discussion

The mobility of an OFET will be influenced by many factors including the thin film morphology, crystallinity, and crystal packing. All films examined here have shown a high degree of crystallinity evidenced by the well-defined 2D GIWAXS patterns, thus changes in morphology and crystal packing are likely to be most important in explaining the mobility trends. For a given crystal packing, uniform films with a high degree of texture and large grains should promote a high mobility, as is seen for the case of NDI-C8 and NDI-C12. Films which exhibit a high degree of mosaicity where crystallites exhibit a large spread in crystal orientations will reduce charge mobility and promote charge trapping. Changes in the side-chain length and type lead to differences in molecular packing as seen by the changes in the size of the *a*-axis and *b*-axis of the unit cells. Changes in the lateral offset of the NDI core in particular can have a large effect on charge transport mobility by modulating the transfer integral. This was indeed found to be the case by Ma et al. who calculated the charge transfer

integral for NDI-C4, NDI-C5, NDI-C6, NDI-C12 as well as NDI-C14 based on their calculated molecular packings [32]. For this series of molecules they calculated that the mobility should decrease with increasing linear chain length due to changes in the displaced stacking of the NDI molecules along the short axis of the molecular plane. That is, changes in $d_S$ (which are correlated with changes in the size of the *b*-axis measured here) were found to mediate significant changes in transfer integral and hence mobility. NDI-C4 was predicted to have the highest charge transport mobility based on its more favourable lateral displacement of NDI cores. However in our case we find that both NDI-C4 and NDI-C12 can exhibit similar charge transport mobilities. We attribute this observation to the competing influence of molecular packing and molecular order. Longer side chains have been found to promote films with superior morphology characterised by larger domain sizes and higher degree of orientational order. For shorter side chains the mobility decreases due to increasing structural disorder, but then increases due to the more favourable crystal packing of NDI-C4 and NDI-C5 that facilitate a larger transfer integral. The difference in the mobility of spin-coated (0.07 $cm^2/Vs$) and blade-coated (0.18 $cm^2/Vs$) films of NDI-C4 in particular is quite stark which can be attributed to high degree of orientational disorder in the spin-coated film, with the AFM image of spin-coated NDI-C4 containing crystallites that possess a high degree of orientational mismatch. A similar large difference between the mobility of spin-coated (0.014 $cm^2/Vs$) and blade-coated (0.060 $cm^2/Vs$) NDI-C6 OFETs is also found with the spin-coated films of NDI-C6 exhibiting quite large orientational disorder compared to blade-coated films. For samples with similar orientation order in spin-coated and blade-coated films (judged by the uniformity of the AFM images and texture seen in the GIWAXS images) such as NDI-C5, NDI-C8 and NDI-C12, similar mobilities for spin-coated and blade-coated OFETs are seen.

Interestingly the branched ethyl-hexyl side chains produced some of the lowest mobilities for this series of molecules. Branched ethyl-hexyl side chains are commonly used for enabling solution processability of organic semiconductors, however these were not found to facilitate optimal film morphologies. This study suggests that longer, linear side chains should be favoured for producing uniform thin films from solution. Long chains also seem to promote a strong edge-on orientation of the NDI core within the unit cell. While such an edge-on orientation may not necessarily lead to improved charge transfer integrals, it is interesting to note that changing the side-chain length can be used to strongly modulate molecular orientation in solution-coated NDI films. Although not commented upon above, strong dichroism in the NEXAFS spectra was also observed in the 1s $\rightarrow \sigma^*$ transitions of NDI-C8 and NDI-C12 indicating molecular ordering of the linear side chains as well as strong orientation of the NDI core.

**5. Conclusions**

We have studied the effect of side-chain length and type on the thin film microstructure and performance of OFETs based on solution-processed NDI molecules. Electron mobilities of ~ 0.2 $cm^2/Vs$ could be achieved for both short (NDI-C4) and long (NDI-C12) linear chains, with lower mobilities observed for intermediate chain lengths. We have interpreted the observed mobility trends in terms of the competing factors of film uniformity and crystal packing, with short side chains promoting a more favourable lateral stacking of NDI units within the unit cell and longer side chains promoting a more uniform thin film morphology. Good correlation was seen between thin film microstructure and OFET mobility, with films with higher degrees of texture, higher uniformity and larger grain sizes in general showing higher mobilities. Systematic increases in the molecular orientation of the NDI core were also seen with increasing side chain length. The use of a branched side chain

in the form of ethyl-hexyl side chain was found to produce lower mobilities and less ordered structures compared to C8 and C12 linear side chains.

**Acknowledgements**

Part of this research was performed at soft X-ray and SAXS/WAXS beamlines at Australian Synchrotron, part of ANSTO. This work was also performed in part at the Melbourne Centre for Nanofabrication (MCN) in the Victorian Node of the Australian National Fabrication Facility (ANFF). Financial support from the Australian Research Council through the Discovery Grant Scheme (DP170102145) is gratefully acknowledged.

**References**

[1] H. Sirringhaus, M. Ando, Materials Challenges and Applications of Solution-Processed Organic Field-Effect Transistors, MRS Bulletin, 33 (2008) 676 - 682.
[2] K.-J. Baeg, M. Caironi, Y.-Y. Noh, Toward Printed Integrated Circuits based on Unipolar or Ambipolar Polymer Semiconductors, Adv. Mater., 25 (2013) 4210-4244.
[3] C.-a. Di, F. Zhang, D. Zhu, Multi-Functional Integration of Organic Field-Effect Transistors (OFETs): Advances and Perspectives, Adv. Mater., 25 (2013) 313-330.
[4] H. Li, W. Shi, J. Song, H.-J. Jang, J. Dailey, J. Yu, H.E. Katz, Chemical and Biomolecule Sensing with Organic Field-Effect Transistors, Chem. Rev., 119 (2019) 3-35.
[5] S.-C. Lo, P.L. Burn, Development of Dendrimers: Macromolecules for Use in Organic Light-Emitting Diodes and Solar Cells, Chemical Reviews, 107 (2007) 1097-1116.
[6] Z. Liu, G. Zhang, D. Zhang, Modification of Side Chains of Conjugated Molecules and Polymers for Charge Mobility Enhancement and Sensing Functionality, Acc. Chem. Res., 51 (2018) 1422-1432.
[7] J. Mei, Z. Bao, Side Chain Engineering in Solution-Processable Conjugated Polymers, Chemistry of Materials, 26 (2014) 604-615.
[8] R.J. Kline, D.M. DeLongchamp, D.A. Fischer, E.K. Lin, L.J. Richter, M.L. Chabinyc, M.F. Toney, M. Heeney, I. McCulloch, Critical Role of Side-Chain Attachment Density on the Order and Device Performance of Polythiophenes, Macromolecules, 40 (2007) 7960-7965.
[9] L. Yang, H. Zhou, W. You, Quantitatively Analyzing the Influence of Side Chains on Photovoltaic Properties of Polymer−Fullerene Solar Cells, The Journal of Physical Chemistry C, 114 (2010) 16793-16800.
[10] J. Mei, Z. Bao, Side Chain Engineering in Solution-Processable Conjugated Polymers, Chem. Mater., 26 (2013) 604-615.
[11] I. Kang, H.-J. Yun, D.S. Chung, S.-K. Kwon, Y.-H. Kim, Record High Hole Mobility in Polymer Semiconductors via Side-Chain Engineering, Journal of the American Chemical Society, 135 (2013) 14896-14899.

[12] J. Lee, A.R. Han, H. Yu, T.J. Shin, C. Yang, J.H. Oh, Boosting the Ambipolar Performance of Solution-Processable Polymer Semiconductors via Hybrid Side-Chain Engineering, Journal of the American Chemical Society, 135 (2013) 9540-9547.
[13] C. Zhang, Y. Zang, F. Zhang, Y. Diao, C.R. McNeill, C.-a. Di, X. Zhu, D. Zhu, Pursuing High-Mobility n-Type Organic Semiconductors by Combination of "Molecule-Framework" and "Side-Chain" Engineering, Adv Mater, 28 (2016) 8456-8462.
[14] M. Halik, H. Klauk, U. Zschieschang, G. Schmid, S. Ponomarenko, S. Kirchmeyer, W. Weber, Relationship Between Molecular Structure and Electrical Performance of Oligothiophene Organic Thin Film Transistors, Advanced Materials, 15 (2003) 917-922.
[15] X. Zhan, A. Facchetti, S. Barlow, T.J. Marks, M.A. Ratner, M.R. Wasielewski, S.R. Marder, Rylene and Related Diimides for Organic Electronics, Adv. Mater., 23 (2011) 268-284.
[16] T. He, M. Stolte, F. Würthner, Air-Stable n-Channel Organic Single Crystal Field-Effect Transistors Based on Microribbons of Core-Chlorinated Naphthalene Diimide, Advanced Materials, 25 (2013) 6951-6955.
[17] X. Gao, C.-a. Di, Y. Hu, X. Yang, H. Fan, F. Zhang, Y. Liu, H. Li, D. Zhu, Core-Expanded Naphthalene Diimides Fused with 2-(1,3-Dithiol-2-Ylidene)Malonitrile Groups for High-Performance, Ambient-Stable, Solution-Processed n-Channel Organic Thin Film Transistors, J. Am. Chem. Soc., 132 (2010) 3697-3699.
[18] H. Yan, Z. Chen, Y. Zheng, C. Newman, J.R. Quinn, F. Dötz, M. Kastler, A. Facchetti, A high-mobility electron-transporting polymer for printed transistors, Nature, 457 (2009) 679 - 687.
[19] D. Shukla, S.F. Nelson, D.C. Freeman, M. Rajeswaran, W.G. Ahearn, D.M. Meyer, J.T. Carey, Thin-Film Morphology Control in Naphthalene-Diimide-Based Semiconductors: High Mobility n-Type Semiconductor for Organic Thin-Film Transistors, Chem. Mater., 20 (2008) 7486-7491.
[20] F. Zhang, Y. Hu, T. Schuettfort, C.-a. Di, X. Gao, C.R. McNeill, L. Thomsen, S.C.B. Mannsfeld, W. Yuan, H. Sirringhaus, D. Zhu, Critical Role of Alkyl Chain Branching of Organic Semiconductors in Enabling Solution-Processed N-Channel Organic Thin-Film Transistors with Mobility of up to 3.50 cm2 V–1 s–1, J. Am. Chem. Soc., 135 (2013) 2338-2349.
[21] W.-Y. Lee, J.H. Oh, S.-L. Suraru, W.-C. Chen, F. Würthner, Z. Bao, High-Mobility Air-Stable Solution-Shear-Processed n-Channel Organic Transistors Based on Core-Chlorinated Naphthalene Diimides, Advanced Functional Materials, 21 (2011) 4173-4181.
[22] M. Ichikawa, Y. Yokota, H.-G. Jeon, G.d.R. Banoukepa, N. Hirata, N. Oguma, Comparative study of soluble naphthalene diimide derivatives bearing long alkyl chains as n-type organic thin-film transistor materials, Org. Electron., 14 (2013) 516-522.
[23] I. Tszydel, M. Kucinska, T. Marszalek, R. Rybakiewicz, A. Nosal, J. Jung, M. Gazicki-Lipman, C. Pitsalidis, C. Gravalidis, S. Logothetidis, M. Zagorska, J. Ulanski, High-Mobility and Low Turn-On Voltage n-Channel OTFTs Based on a Solution-Processable Derivative of Naphthalene Bisimide, Adv. Funct. Mater., 22 (2012) 3840-3844.
[24] H.E. Katz, J. Johnson, A.J. Lovinger, W. Li, Naphthalenetetracarboxylic Diimide-Based n-Channel Transistor Semiconductors: Structural Variation and Thiol-Enhanced Gold Contacts, Journal of the American Chemical Society, 122 (2000) 7787-7792.
[25] H.E. Katz, T. Siegrist, J.H. Schön, C. Kloc, B. Batlogg, A.J. Lovinger, J. Johnson, Solid-State Structural and Electrical Characterization of N-Benzyl and N-Alkyl Naphthalene 1,4,5,8-Tetracarboxylic Diimides, ChemPhysChem, 2 (2001) 167-172.
[26] T. Kakinuma, H. Kojima, M. Ashizawa, H. Matsumoto, T. Mori, Correlation of mobility and molecular packing in organic transistors based on cycloalkyl naphthalene diimides, Journal of Materials Chemistry C, 1 (2013) 5395-5401.
[27] A. Dey, A. Kalita, P. Krishnan Iyer, High-Performance n-Channel Organic Thin-Film Transistor Based on Naphthalene Diimide, ACS Applied Materials & Interfaces, 6 (2014) 12295-12301.
[28] N.B. Kolhe, R.N. Devi, S.P. Senanayak, B. Jancy, K.S. Narayan, S.K. Asha, Structure engineering of naphthalene diimides for improved charge carrier mobility: self-assembly by hydrogen bonding, good or bad?, Journal of Materials Chemistry, 22 (2012) 15235-15246.

[29] H.E. Katz, A.J. Lovinger, J. Johnson, C. Kloc, T. Siegrist, W. Li, Y.Y. Lin, A. Dodabalapur, A soluble and air-stable organic semiconductor with high electron mobility, Nature, 404 (2000) 478.
[30] T.B. Singh, S. Erten, S. Günes, C. Zafer, G. Turkmen, B. Kuban, Y. Teoman, N.S. Sariciftci, S. Icli, Soluble derivatives of perylene and naphthalene diimide for n-channel organic field-effect transistors, Organic Electronics, 7 (2006) 480-489.
[31] D. Shukla, S.F. Nelson, D.C. Freeman, M. Rajeswaran, W.G. Ahearn, D.M. Meyer, J.T. Carey, Thin-Film Morphology Control in Naphthalene-Diimide-Based Semiconductors: High Mobility n-Type Semiconductor for Organic Thin-Film Transistors, Chemistry of Materials, 20 (2008) 7486-7491.
[32] Z. Ma, H. Geng, D. Wang, Z. Shuai, Influence of alkyl side-chain length on the carrier mobility in organic semiconductors: herringbone vs. pi–pi stacking, Journal of Materials Chemistry C, 4 (2016) 4546-4555.
[33] S. Maniam, S. Sandanayake, E.I. Izgorodina, S.J. Langford, Unusual Products from Oxidation of Naphthalene Diimides, Asian Journal of Organic Chemistry, 5 (2016) 490-493.
[34] A. Welford, S. Maniam, E. Gann, L. Thomsen, S.J. Langford, C.R. McNeill, Thionation of naphthalene diimide molecules: Thin-film microstructure and transistor performance, Organic Electronics, 53 (2018) 287-295.
[35] H. Zhou, Q. Chen, G. Li, S. Luo, T.-b. Song, H.-S. Duan, Z. Hong, J. You, Y. Liu, Y. Yang, Interface engineering of highly efficient perovskite solar cells, Science, 345 (2014) 542-546.
[36] C.M. Stafford, K.E. Roskov, T.H. Epps, III, M.J. Fasolka, Generating thickness gradients of thin polymer films via flow coating, Rev. Sci. Instrum., 77 (2006) 023908.
[37] N.M. Kirby, S.T. Mudie, A.M. Hawley, D.J. Cookson, H.D.T. Mertens, N. Cowieson, V. Samardzic-Boban, A low-background-intensity focusing small-angle X-ray scattering undulator beamline, J. Appl. Cryst., 46 (2013) 1670-1680.
[38] I. Ilavsky, Nika - software for 2D data reduction, J. Appl. Cryst., 45 (2012) 324-328.
[39] B.C.C. Cowie, A. Tadich, L. Thomsen, The Current Performance of the Wide Range (90--2500 eV) Soft X-ray Beamline at the Australian Synchrotron, AIP Conf. Proc., 1234 (2010) 307-310.
[40] E. Gann, C.R. McNeill, A. Tadich, B.C.C. Cowie, L. Thomsen, Quick AS NEXAFS Tool (QANT): A program for NEXAFS loading and analysis developed at the Australian Synchrotron, J. Synchrotron Rad., 23 (2016) 374-380.
[41] M.M. Nahid, E. Gann, L. Thomsen, C.R. McNeill, NEXAFS spectroscopy of conjugated polymers, Eur. Polym. J., 81 (2016) 532–554.
[42] F. Tao, S.L. Bernasek, Understanding Odd−Even Effects in Organic Self-Assembled Monolayers, Chem. Rev., 107 (2007) 1408-1453.
[43] P.M. Alvey, J.J. Reczek, V. Lynch, B.L. Iverson, A Systematic Study of Thermochromic Aromatic Donor−Acceptor Materials, J. Org. Chem., 75 (2010) 7682-7690.
[44] S.C.B. Mannsfeld, A. Virkar, C. Reese, M.F. Toney, Z. Bao, Precise Structure of Pentacene Monolayers on Amorphous Silicon Oxide and Relation to Charge Transport, Adv. Mater., 21 (2009) 2294-2298.
[45] C.R. McNeill, H. Ade, Soft X-ray characterisation of organic semiconductor films, J. Mater. Chem. C, 1 (2013) 187-201.

**Graphical Abstract**

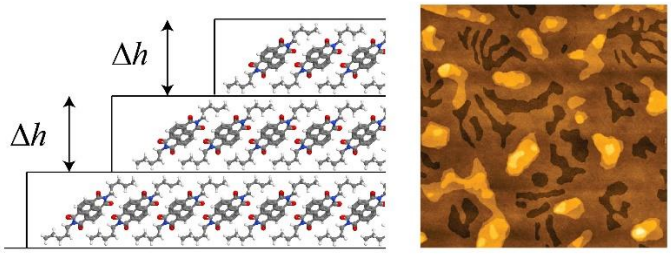

**Supplementary data for**

Influence of alkyl side-chain type and length on the thin film microstructure and OFET performance of naphthalene diimide-based organic semiconductors

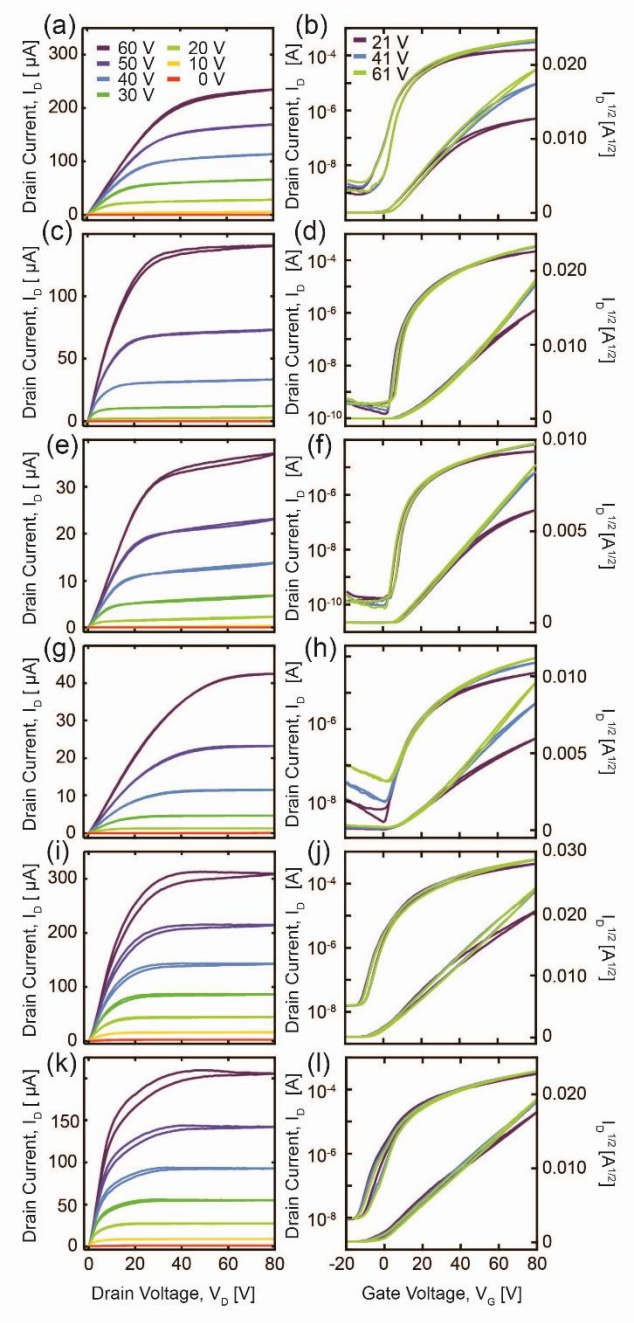


Figure S1. Output (a, c, e, g, i, k) and transfer (b, d, f, h, j, l) of spin-coated OFETs based on NDI-C4, (a, b), NDI-C5, (c, d), NDI-C6, (e, f), NDI-EH, (g, h), NDI-8H, (i, j), and NDI-C12, (k, l).